

Effect of hydrogen on plastic strain localization and fracture of steels

This content has been downloaded from IOPscience. Please scroll down to see the full text.

2016 IOP Conf. Ser.: Mater. Sci. Eng. 116 012024

(<http://iopscience.iop.org/1757-899X/116/1/012024>)

View [the table of contents for this issue](#), or go to the [journal homepage](#) for more

Download details:

IP Address: 84.237.1.97

This content was downloaded on 09/03/2016 at 10:33

Please note that [terms and conditions apply](#).

Effect of hydrogen on plastic strain localization and fracture of steels

M V Nadjozhkin¹, A G Lunev¹, Yu V Li¹, S A Barannikova^{1,2,3}

¹ Institute of Strength Physics and Materials Science, SB RAS, Tomsk, 634055, Russia

² Tomsk State University, Tomsk, 634050, Russia

³ Tomsk State University of Architecture and Building, Tomsk, 634003, Russia

E-mail: bsa@ispms.tsc.ru

Abstract. The effect of interstitial hydrogen atoms on the mechanical properties and plastic strain localization patterns in tensile tested specimens of low-carbon steels have been studied using a double exposure speckle photography technique. It is found that the mechanical properties of low-carbon steels are affected adversely by hydrogen embrittlement. The deformation diagrams were examined for the deformed samples of low-carbon steels. These are found to show all the plastic flow stages: the linear, parabolic and pre-failure stages would occur for the respective values of the exponent n from the Ludwik-Holomon equation.

1. Introduction

Previously, we presented experimental data in [1] according to which plastic strain development in solids exhibited a localized character over the entire process. This phenomenon is especially clearly manifested on a macroscopic scale, where the patterns of strain localization are related to the deformation hardening operative on the corresponding stages of straining. Embrittlement due to hydrogen (H) involves a vast loss of mechanical properties with the following characteristics such as, for example, decrease of ductility and fracture tension with the increase of H concentration. As is pointed out in [2, 3], this phenomenon poses a serious practical problem, the solution of which determines the durability and safety of operation of a steel structure.

It was established in [4, 5] that the significant progress in understanding of Hydrogen-Enhanced Localized Plasticity (HELP) mechanism has been recently achieved in studies based on the so-called hydrogen-induced localized softening effect. Main idea of this approach takes into consideration material softening in micro-scale caused by enhanced dislocation mobility in the presence of hydrogen. This phenomenon has been evidenced in a variety of metals with different types of dislocations [6]. The main aim of this investigation was to elucidate the effect of dissolved hydrogen on the macroscopic plastic flow localization patterns in tensile strained steels.

2. Experimental details

The investigations were performed for polycrystals of low-carbon steel (Fe-0.07%C). The samples had a working part with dimensions of 50·5·1 mm and were tensile strained at 300 K on an Instron Model 1185 testing machine at a mobile clamp velocity of 8.3·10⁻⁶ m/s. The loading curves of the tested materials are illustrated in Fig. 1. The method for studying the hydrogen diffusivity and the interaction of hydrogen with lattice defects was proposed in [7]. Based on these observation, the steel samples were electrolytically saturated with hydrogen in a thermostatted three-electrode electrochemical cell



with graphite anode, operating at a controlled constant cathode potential of $U = -600$ mV (relative to silver chloride reference electrode) in a 1 N sulfuric acid solution containing 20 mg/l thiourea. The hydrogenation was effected at 323 K for 24 h after preliminary purging the solution with nitrogen. The current–voltage curves were recorded using an IPC-Compact potentiostat. Prior to mechanical testing, the samples were kept in liquid nitrogen.

The stress-strain diagram was obtained simultaneously with measuring the fields of the displacement vectors $\mathbf{r}(x, y)$ with the aid of double-exposure speckle photography (DESP) technique. A special device was also designed in [1]; it had field of vision ~ 100 mm; spatial resolution comparable to optical microscopy $\sim 1\text{--}2$ μm and real-time mode of operation. This enabled reconstruction of displacement vector fields $\mathbf{r}(x, y)$ for the sample surface. On the base of this data, the plastic distortion tensor is evaluated for the deforming sample in the coordinates x, y and z , i.e. longitudinal (ε_{xx}), transverse (ε_{yy}), shear ($\varepsilon_{xy} = \varepsilon_{yx}$) and rotation (ω_z) components. This technique can visualize localized plastic flow nuclei, using the spatial distributions of plastic distortion tensor components; the kinetics of nuclei motion can be determined from the temporal evolution of nuclei.

3. Experimental results

We have studied the evolution of patterns of the plastic flow macrolocalization in low-carbon steel polycrystals in the initial state and upon the saturation of the electrolytic with hydrogen.

The stress–strain (σ – ε) curve of plastic flow measured in tension for low-carbon steel polycrystals in the initial (hydrogen-free) state, exhibit a tooth and a flow trough (I) that extends up to $\varepsilon_{\text{tot}} = 0.04$ and is followed by the stages of (II) linear deformation hardening with a constant coefficient of $\theta_{\text{II}} \approx 920$ MPa; (III) parabolic (Taylor's) hardening with a power index of $n = 1/2$ and (IV) prefracture with $n < 1/2$, which extends up to $\varepsilon_{\text{tot}} = 0.42$ (Figure 1, curve 1).

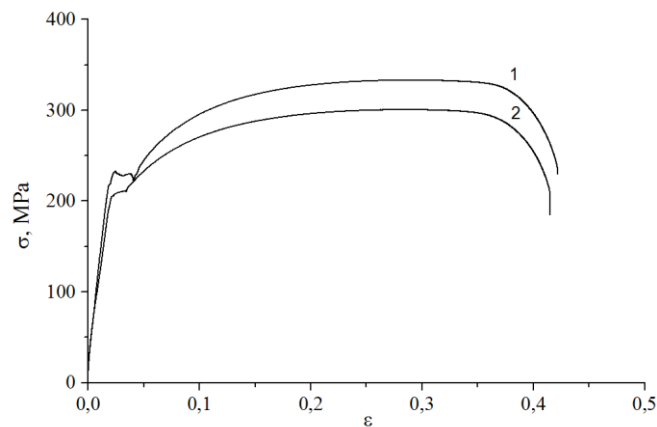


Figure 1. The flow curves of low-carbon steel polycrystals (a): 1 – free of interstitial impurity atoms and 2 – upon the electrolytic saturation with hydrogen at $U = -600$ mV in 1 N aqueous H_2SO_4 for 24 h at $T = 323$ K

The $\sigma(\varepsilon)$ curves of low-carbon steel polycrystals saturated with hydrogen exhibit a flow trough (I) with a constant coefficient of $\theta_{\text{I}} \approx 450$ MPa that extends up to $\varepsilon_{\text{tot}} = 0.05$ and is followed by the stages of (II) linear deformation hardening with a constant coefficient of $\theta_{\text{II}} \approx 730$ MPa; (III) parabolic (Taylor's) hardening with a power index of $n = 1/2$; and (IV) prefracture with $n < 1/2$, which extends up to $\varepsilon_{\text{tot}} = 0.41$ (Figure 1, curve 2). The entire plastic flow curve shifts downward relative to that for the low-carbon steel polycrystals in the initial (hydrogen-free) state. Thus, the hydrogenation of low-carbon steel polycrystals led to a decrease in the yield and strength stresses.

The measurements of local strain distributions using the DESP method showed that the strain is macroscopically localized at all stages of plastic flow in low-carbon steel polycrystals. At the yield

plateau Lüders band propagation is observed which separated the strained and unstrained parts of the sample. An analysis of these patterns revealed that, in the initial (hydrogen-free) state of polycrystals, the tensile plastic strain at the stage of yield plateau (I) in the deforming material there travels four solitary fronts of plastic deformation at different constant rates $V_{aw} \sim 10^{-5}$ m/s (Figure 2a).

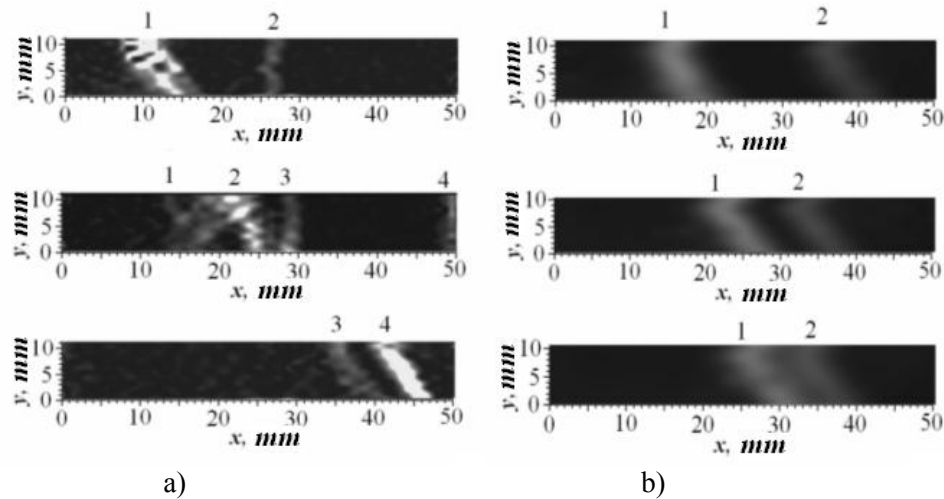


Figure 2. Pattern of strain distribution at the yield plateau (I) in low-carbon steel polycrystals in the initial state (free of interstitial impurity atoms) (a) and upon the electrolytic saturation with hydrogen at $U = -600$ mV in 1 N aqueous H_2SO_4 for 24 h at $T = 323$ K (b) at a total strain of $\epsilon_{tot} = 0.005 \dots 0.03$

The tensile plastic strain at the stage of linear deformation hardening (II) is concentrated within local zones spaced by a distance of $\lambda = 8 \pm 1$ mm (Figure 3a). These local strain zones (autowaves) moved at a velocity of $5.3 \cdot 10^{-5}$ m/s, which was determined from the slope of the $X(t)$ curves that plot the positions X of maxima of the ϵ_{xx} strain component on the axis of straining as functions of time t . At the stage of parabolic deformation hardening (III), the system of equidistant strain localization zones becomes stationary, then these immobile foci of plastic strain localization start to move consistently with a tendency to merge together at the middle of a sample, where the fracture takes place (Figure 4 a).

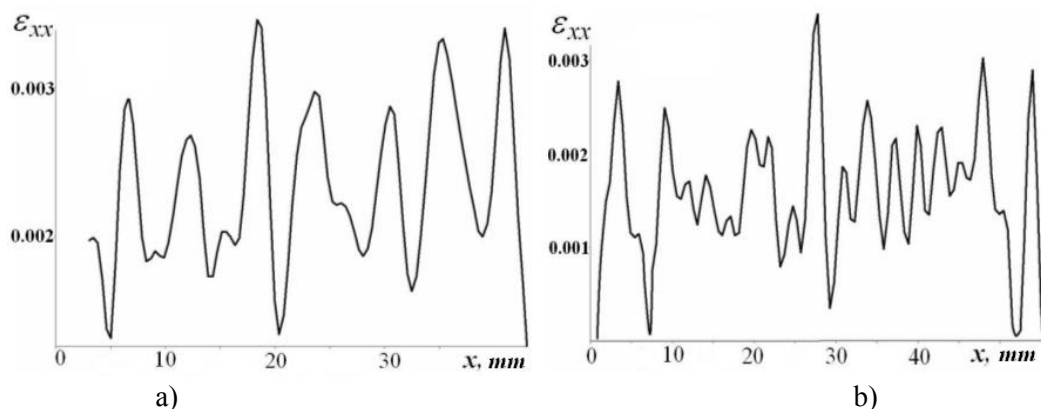


Figure 3. Pattern of strain distribution plotted as the local elongation component $\epsilon_{xx}(x)$ along axis of tension at stage of linear deformation hardening (II) in low-carbon steel polycrystals in the initial state (free of interstitial impurity atoms) at a total strain of $\epsilon_{tot} = 0.067$ (a) and upon the electrolytic saturation with hydrogen at $U = -600$ mV in 1 N aqueous H_2SO_4 for 24 h at $T = 323$ K at a total strain of $\epsilon_{tot} = 0.075$ (b)

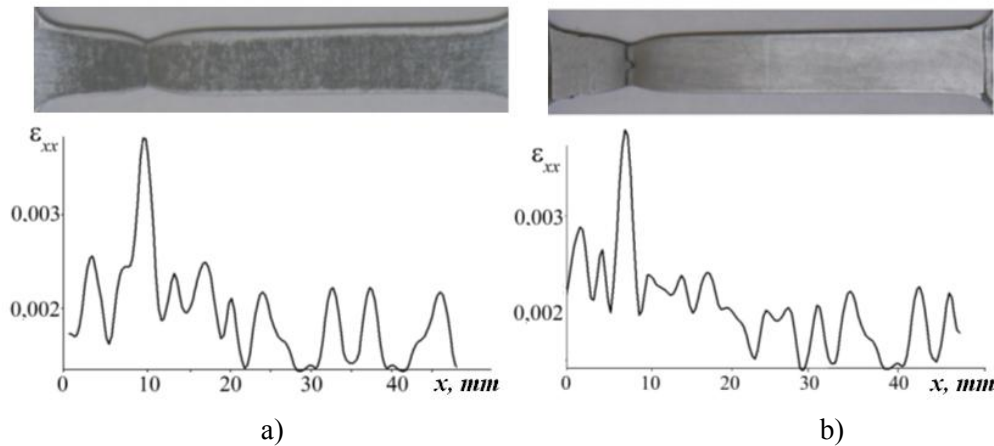


Figure 4. Pattern of strain distribution plotted as the local elongation component $\epsilon_{xx}(x)$ along axis of tension at the prefracture stage (IV) in low-carbon steel polycrystals in the initial state (free of interstitial impurity atoms) at a total strain of $\epsilon_{tot} = 0.36$ (a) and upon the electrolytic saturation with hydrogen at $U = -600$ mV in 1 N aqueous H_2SO_4 for 24 h at $T = 323$ K at a total strain of $\epsilon_{tot} = 0.35$ (b)

An analysis of the distributions of local strain ϵ_{xx} in tensile tested low-carbon steel polycrystals saturated hydrogen showed that, in this case at the flow trough (I) with a constant coefficient of $\theta_1 \approx 450$ MPa in the material there emerge two deformation fronts moving in opposite directions (Figure 2b). The fronts' motion rates are $1.4 \cdot 10^{-4}$ and $5.5 \cdot 10^{-5}$ m/s. The point, at which the fronts meet, marks off the end of stage I. At the stage of linear deformation hardening (II), the pattern of plastic strain localization represented a set of wide zones, each of which contains two to three related local strain foci. The zones exhibited a characteristic spacing $\lambda = 6.0 \pm 1$ mm (Figure 3b). These local straining zones (autowaves) also moved at a velocity of $8.3 \cdot 10^{-5}$ m/s. At the stage of parabolic deformation hardening (III), the system of strain localization zones became stationary. At the prefracture stage (IV), the immobile foci of plastic strain localization started moving consistently with a tendency to merge into a high-amplitude focus of localized straining (Figure 4 b), where a neck-like narrowing of the sample cross section was formed. According to [8] in the course of deformation the space-time periodic pattern of nuclei is finally replaced by a single localized plasticity nucleus for single crystals of Fe-18Cr-12Ni-2Mo austenite steel upon the electrolytic saturation with hydrogen.

4. Conclusion

Thus, we have elucidated the effect of hydrogen on the macroscopic patterns of plastic strain localization in tensile tested polycrystals of low-carbon steel ($Fe-0.07\%C$). It is established that the hydrogenation enhances the localization of straining leads to significant changes in the characteristics distances between local straining zones. According to [5] it can be a result of interdislocation interactions and the generation of defects. The mechanism of hydrogen-stimulated plastic strain localization is still under discussion. Therefore, the wave patterns of localized plasticity appear to be useful for a detailed analysis of plasticity exhibited by real metals and alloys. The examination of localized deformation patterns suggests that the location and time of future fracture can be determined long before a macroscopic neck forms in the test sample.

Acknowledgement

The work was performed in the frame of the Tomsk State University Academic D.I. Mendeleev Fund Program and the Program of Fundamental Research of State Academies of Sciences for the period 2013-2020 yrs.

References

- [1] Zuev L B, Danilov V I, Barannikova S A, Gorbatenko V V 2009 *Phys. Wave Phen.* **17** 1
- [2] Hirth J P 1980 *Met. Mat. Trans. A* **11** 861
- [3] Ramunni V P, De Paiva Coelho T, de Miranda P E V 2006 *Mat. Sci. Eng. A* **435–436** 504
- [4] Birnbaum H K, Sofronis P 1994 *Mat. Sci. Eng. A* **176** 191
- [5] Sofronis P, Liang Y, Aravas N 2001 *Eur. J. Mech. A: Sol.* **20** 857
- [6] Robertson I M 2001 *Eng. Frac. Mech.* **68** 671
- [7] Yagodzinskyy Y, Todoshchenko O, Papula S, Hänninen H 2011 *Steel Res. Int.* **82** 20
- [8] Barannikova S A, Nadezhkin M V, Mel' nichuk V A, Zuev L B 2011 *Tech. Phys. Lett.* **37** 793